Tuftelin1 Drives Experimental Pulmonary Fibrosis Progression by Facilitating Stress Fiber Assembly

Caoyuan Niu
Henan Normal University
Kai Xu
Henan Normal University
Yanan Hu
the Third Affiliated Hospital of Xinxiang Medical University
Yanling Jia
Henan Normal University
Xiaoyue Pan
Henan Normal University
Ruyan Wan
Henan Normal University
Hui Lian
Henan Normal University
Qiwen Wang
Henan Normal University
Lan Wang
Henan Normal University
Juntang Yang
Henan Normal University
Yajun Li
Henan Normal University
Ivan Rosas
Henan Normal University
Guoying Yu (guoyingyu@htu.edu.cn)
Henan Normal University

Research Article

Keywords: IPF, TUFT1, Stress fiber, Bleomycin, N-WASP

Posted Date: September 14th, 2023

DOI: https://doi.org/10.21203/rs.3.rs-3341977/v1

Additional Declarations: No competing interests reported.

Version of Record: A version of this preprint was published at Respiratory Research on December 17th, 2023. See the published version at https://doi.org/10.1186/s12931-023-02633-w.

Abstract

Idiopathic pulmonary fibrosis (IPF) is a progressive interstitial lung disease (ILD) with unknown etiology, characterized by sustained damage repair of epithelial cells and abnormal activation of fibroblasts. However, the underlying mechanism of the disease remains elusive. This study was designed to evaluate the role of Tuftelin1 (TUFT1) in IPF and elucidate its molecular mechanism. We investigated the level of TUFT1 in the IPF and bleomycin-induced mouse models and explored the influence of TUFT1 deficiency on pulmonary fibrosis. Additionally, we explored the effect of TUFT1 on cytoskeleton and illustrated the relationship between stress fiber and pulmonary fibrosis. Our results demonstrated a significant upregulation of TUFT1 in IPF and the bleomycin-induced fibrosis model. Disruption of TUFT1 exerted inhibitory effects on pulmonary fibrosis in both in vivo and in vitro settings. Moreover, TUFT1 facilitated the assembly of microfilaments in A549 and MRC-5 cells, with a pronounced association between TUFT1 and N-WASP observed during microfilament formation. Meanwhile TUFT1 can promote the phosphorylation of tyrosine residue 256 (Y256) of the Neuronal Wiskott-Aldrich syndrome protein (p^{Y256}N-WASP). Furthermore, TUFT1 promoted TGF-β1 induced fibroblast activation by increasing nuclear translocation of p^{Y256}N-WASP in fibroblasts, while wiskostatin, a N-WASP inhibitor, suppressed these processes. Our findings suggested TUFT1 plays an important role in pulmonary fibrosis via its influence on stress fiber, and blockade of TUFT1 effectively reduces pro-fibrotic phenotypes. Pharmacological targeting of the TUFT1-N-WASP axis may represent a promising therapeutic approach for pulmonary fibrosis.

1 Introduction

Idiopathic pulmonary fibrosis (IPF) is a progressive, chronic, and ultimately fatal interstitial lung disease characterized by enhanced extracellular matrix deposition, repetitive alveolar epithelial injury, dysregulated wound repair and fibroblasts activation[1, 2]. The median survival of IPF patients without transplant is estimated to be only 2–4 years [3, 4]. Currently, therapeutic choices for IPF remain constrained, with only FDA approved drugs pirfenidone and nintedanib demonstrating the capacity to modestly decelerate disease progression [5, 6]. Hence, the pursuit of novel preventative and therapeutic modalities stands as a pressing priority in addressing this ailment.

IPF was thought to a result of multiple genetic and environmental risk factors [7–9]. Identifying the molecular mechanisms underlying the disease and potential prognostic biomarkers is critical for developing effective treatments. In a previous study, a hybrid feature selection method was employed to extract informative genes, with TUFT1 identified as a candidate gene for IPF, while its role in IPF was still unclear [10].

TUFT1 was an acidic protein mainly synthesized by ameloblasts, and it plays an essential role in developing and mineralizing tooth tissues [11, 12]. However, it is also expressed in non-mineralizing tissues and has been shown to promote cell proliferation and migration in renal cell carcinoma and metastasis in triple-negative breast cancer and pancreatic cancer [13–15]. Moreover, TUFT1 is regulated

by hypoxia and the Hedgehog signaling pathway and is involved in multiple diseases. In NCI-H441 lung adenocarcinoma cells, TUFT1 was shown to be a novel target of TGF-β1 and exhibited a pivotal involvement in the orchestration of microfilament formation within A549 cells [16].

IPF is characterized by the remodeling of the actin cytoskeleton of epithelial cells, fibroblasts and endothelial cells[17]. The actin cytoskeleton is a complex, dynamic biopolymer network that performs essential functions in cell migration, cell interaction with the environment, and mechanical properties of the cell surface [18–22]. N-WASP is an actin nucleation factor that promotes polymerization of branched actin filaments [23]. The activation of N-WASP is regulated by the phosphorylation of tyrosine residue 256 (Y256), which is mediated by TGF-β1[24].

Here, we investigated the role of TUFT1 in IPF. Our results showed TUFT1 is increased in IPF and bleomycin-induced pulmonary fibrosis. Suppressing TUFT1 inhibits bleomycin-induced mouse pulmonary fibrosis. Mechanistically, suppressing TUFT1 inhibited pro-fibrotic phenotypes in vitro by down-regulating the expression of p^{Y256}N-WASP and impeding the formation of stress fiber, while TUFT1 overexpression promoted the assembling of the actin filaments. Furthermore, we found that TUFT1 attracted p^{Y256}N-WASP around the nucleus, and this phenomenon could be suppressed by wiskostatin, an N-WASP inhibitor. These finding implicated that TUFT1 plays an important role in the activation of N-WASP and in the formation of cytoskeleton, and it may represent a promising therapeutic target for IPF.

2 Materials and methods

2.1 Reagents and antibodies

Recombinant human TGF-β1 was obtained from R&D systems (Minneapolis, MN, USA). Bleomycin sulfate was obtained from Hisun Pharm (Taizhou, China). Sodium orthovanadate was obtained from Sigma-Aldrich (Shanghai, China). Wiskostatin was obtained from Abcam (Shanghai, China). N-WASP was obtained from Proteintech (Wuhan, China). Goat anti-rabbit IgG of β-actin, α-SMA, p^{Y256}N-WASP and GAPDH, were purchased from Affinity Biosciences (Changzhou, China). Goat anti-mouse IgG of Vimentin and E-cadherin were purchased from Cell Signaling Technology (Shanghai, China), Goat anti-rabbit IgG of N-cadherin, Fibronectin and Collagen I were purchased from Cell Signaling Technology (Shanghai, China), TUFT1 was purchased from Thermo Fisher (Suzhou, China).

2.2 Human Lung tissues and the mouse lung fibrosis model induced by bleomycin

Human lung tissues were obtained by surgical lung biopsy (SLB) from patients in Xinxiang central hospital. Wild-type male C57BL/6N mice (9–10 weeks, 19–24 g) were obtained from the Charles River (Beijing, China). Mice were raised in a controlled environment with a cycle of 12-hour light/dark, auto-regulated temperature and humidity, and access to food and water unrestricted. To knock down the Tuft1 gene *in vivo*, Tuft1/shRNA-AAV(5×10^{12} Vg/mL) (HANBIO, Shanghai, China) was administered via

intratracheal injection of adenoviral particles 7 days before the experiment. The control group received vector adenoviral particles (shNC). On day 0, the mice were anesthetized by isoflurane and bleomycin (1.5 U/kg.bw, i.t.) or 0.9% saline (50 μL) was instilled into the trachea. The mice were euthanized and lung samples were collected on day 14.

2.3 Cell culture

The human lung adenocarcinoma cell line A549 (ATCC ® CCL-185™, ATCC, Manassas, VA), negatively tested for mycoplasma, was cultured in DMEM/F12 medium with 10% fetal bovine serum and antibiotics (100 units/mL penicillin and 100 μg/mL streptomycin). The human lung normal fibroblast cell line (MRC-5) was purchased from Procell Life Science &Technology Co., Ltd. (Wuhan, China). MRC-5 was cultured in MEM medium (containing NEAA) (Shanghai Zhong Qiao Xin Zhou Biotechnology Co., Ltd., ZQ-300) with 10% fetal bovine serum and antibiotics (100units/ml penicillin and 100 μg/ml streptomycin) in an atmosphere of 5% CO_2 and humidified at 37°C.

2.4 Small interfering RNA (siRNA) transfection

TUFT1/siRNA-1(5'-GGAGTCCCATGATGGACAT-3'), TUFT1/siRNA-2(5'-GCAGAGGCUGUGUGACAAATT-3'), TUFT1/siRNA-3(5'-GAGGAACTTCGGAGCAACA-3') were purchased from RIBOBIO (Guangzhou, China). To transfect siRNA into A549 and MRC-5 cells, the cells were cultured on 6-wellplates at 50–70% coverage before transfection. Lipofectamine RNAi MAX (RIBOBIO, Guangzhou, China), Opti-MEM (Thermo Fisher) and Individual siRNA (50 nM) were mixed completely and incubated for 5–10 min at room temperature. The efficiency of transfection was testified by western blot in 48 h after transfection.

2.5 Adenovirus generation and infection

The specific shRNA of Tuft1 was obtained from HANBIO (Shanghai, China). Adenovirus generation and subsequent infection were conducted following previously described protocols[25]. Briefly, HEK293T cells were transfected with lipofectamine 3000 (Thermo Fisher Scientific, Shanghai, China) and plasmids to generate adenovirus. The adenovirus-containing medium was collected 48 hours post-transfection and add fresh medium immediately. After another 24 hours, collected the medium again and the adenovirus-containing medium was centrifugated immediately (25,000 rpm, 4°C, 2 hours; Beckman Ti70 rotor). The supernatant was divided into aliquots after aseptic filtration and frozen at -80°C for later use.

2.6 Hydroxyproline assay

Ahydroxyproline assay kit (MAK008, Sigma, St. Louis, MO, USA) was used to detect the content of hydroxyproline in mice right lung [26]. Briefly, the fresh lung tissue was homogenized in water (100 μL water of every 10 mg lung tissue). Hydrolyzed the samples for 3 hours at 120°C. Next, the samples were centrifuged (12,000rpm, 4°C, 3 mins; Beckman Microfuge 20R) and extracted 10 μL supernatant of every sample, the samples were transferred to a 96-well plate and dry them at 56℃. The samples in the plate were incubated for 5 minutes at 20℃ after added 100 μL chloramine T reagent into each well. Afterward, the samples were incubated for 90 min at 56°C after mixed with 100 μL p-dimethylaminobenzaldehyde reagent. Absorbance of samples was measured by BioTek ELx800 plate reader at λ = 560 nm (Winooski,

VT, USA). The hydroxyproline content of samples was calculated by a standard rat tail collagen (Sigma, St. Louis, MO, USA).

2.7 Histological and morphometric analysis

The lungs of mice were collected and fixed with 4% paraformaldehyde. The lung tissues were embedded in paraffin, and the lung tissues would be cut into 3 μm sections for further study on slides. The sections were stained with Masson's trichrome (Beyotime) and H&E (Beyotime) to assess the collagen content and evaluate the morphometric changes. The acquisition of images was performed using a BioTek Cytation C10 Confocal Imaging Reader. Images were analyzed by Image Pro Plus software (version 6.0, Media Cybernetics).

2.8 Immunohistochemical staining

The lung slides were prepared following previously described protocols [27]. The lung sections were incubated with the primary antibodies overnight at 4°C, then the secondary antibody biotinylated anti-rabbit IgG (1:100, Beyotime) was incubated for 60 min at 37°C. Followed by incubating with SABC (1:100, Beyotime), and then visualized by DAB stain (Beyotime).

2.9 Wound-healing assay

SiRNA control or TUFT1 siRNA was transfected into A549 and MRC-5 cells. After 24 hours, the cells were placed in a 6-well plate using a culture medium containing 1% FBS. Upon reaching confluence, a pipette tip was utilized to create a direct scratch across the cell monolayer. Pictures were taken at the predetermined time intervals to document the progression of wound healing. Wound healing is calculated as follows: [1-(Width of the wound at a given time/width of the wound at t = 0)] × 100%.

2.10 Transwell assay

Cell migration assay was performed using a transwell chamber. A549 cells that transfected with SiRNA control or TUFT1 siRNA were seeded into transwell plates with serum-free medium, then medium containing 10% FBS was added to the bottom of the chamber. After 24 hours, Migration cells were fixed and stained with 1% crystal violet and counted in three random fields under an optical microscope.

2.11 Collagen gel contraction assay

Collagen gel contraction assay was performed using a cell contraction assay kit (CBA-201, Cell Biolabs, Inc. (San Diego, CA)). MRC-5 cells were suspended in bovine type 1 collagen solution (chilled on ice) at the concentration of 1.85 mg/mL and seeded at a density of 1×10^6 cells/well in a Costar low attachment surface polystyrene 24-well plate (Corning; Kennebunk, ME). The plate was then placed in a 37°C incubator for 1 h to allow for collagen gel polymerization, and 1 mL of culture medium was added on top of the gel lattice, and cells were incubated overnight. Then cells were pre-incubated with Sodium orthovanadate (20 μM) for 24 hours or Wiskostatin (10 μM) for 1 h. Once the contraction agonists were added, the gels were meticulously detached from the sidewalls of each well by a sterile scalpel.

Photographs were captured after 24 hours, and the analysis of gel disc area was conducted using Image J software for quantification.

2.12 Immunofluorescence staining

The 4% paraformaldehyde was used to fix the lung sections and cell slides and 0.3% Triton X-100 was used to elevate the permeable ability of cells. Then, the sections were block by 10% goat serum for 0.5 h at 37°Cand incubated with primary antibodies overnight at 4°C. Corresponding secondary antibodies were incubated for 1 h at 37°C. F-actin was stained with Phalloidin-iFluor 594 Reagent (ab176757, Abcam, USA) and nuclei were stained with DAPI. The images were captured by a fluorescence microscope (Zeiss LSM780, Carl Zeiss).

2.13 Western blotting

The steps of Western blot analyses were described as previously [28]. Initially, lung homogenates or cell lysates were prepared by RIPA lysis buffer (AR0102, Boster, Wuhan, China). The protein concentrations were detected by BCA kit (Solarbio, Beijing, China). The protein was loaded onto SDS-PAGE as equal amounts and electrotransferred onto PVDF membranes completely. The membranes were incubated with primary antibodies overnight at 4°C and incubated with corresponding secondary antibodies for 1 hour at room temperature. The images were captured by Odyssey Imaging System (LI-COR Biosciences, Lincoln, NE, USA). The densitometry band quantification was measured by the Image Studio software (LI-COR Biosciences, Lincoln, NE, USA).

2.14 Co-Immunoprecipitation (co-IP)

HEK293T cells were lysed in co-immunoprecipitation buffer (AR0107, Boster, Wuhan, China) and incubated for 30 min on ice. The lysate was then centrifuged at 10,000 × *g* for 10 min and the supernatant was collected. The supernatant was incubated with anti-HA beads (Bimake, B26202, Shanghai, China) or anti-Flag beads (B26102, Bimake, Shanghai, China) at 4°C overnight. The beads were washed three times with immunoprecipitation wash buffer (50 mM Tris, 150 mM NaCl, 0.5% Tween 20, pH 7.5) and subjected to further analysis.

2.15 Statistical Analysis

The statistical analysis involved using a two-tailed Student's t-test for comparing two experimental groups. One-way or two-way analysis of variance was used for multi-group comparisons, followed by Tukey's multiple comparison test. Differences were considered statistically significant in all cases when $P < 0.05$.

3 Results

3.1 The expression of TUFT1 was increased in IPF and bleomycin induced pulmonary fibrosis

IHC showed that TUFT1 was increased significantly in IPF lung tissues, and TUFT1 was mainly located in myofibroblasts in the fibroblast foci of the IPF lung (Fig. 1A). Meanwhile we detected the expression of TUFT1 in bleomycin induced fibrotic mouse lung tissues, and found that TUFT1 was increased significantly in BLM-induced fibrotic mouse lungs compared to the control (Fig. 1B-1D). These above data suggested that TUFT1 was associated with pulmonary fibrosis *in vivo*.

To further establish the association between TUFT1 and pulmonary fibrosis in an in vitro context, A549 and MRC-5 cells were exposed to TGF-β1 (5 ng/mL) for a duration of 24 hours. This treatment resulted in a marked reduction in the epithelial marker E-cadherin, coupled with a pronounced elevation in the mesenchymal markers N-cadherin and Vimentin. Furthermore, the protein levels of TUFT1 were notably upregulated in TGF-β1-induced A549 cells (Fig. 1E). Similarly the ECM protein collagen and myofibroblasts marker α-SMA increased in TGF-β1-treated human lung fibroblasts (MRC-5 cells), and the protein levels of TUFT1 were increased in TGF-β1-induced MRC-5 cells (Fig. 1F, G). These results sustain the idea that TUFT1 acts an important role not only in bleomycin-induced fibrosis mice model but also in TGF-β1-treated pulmonary cells.

3.2 Loss of TUFT1 alleviated bleomycin-induced mouse pulmonary fibrosis

To investigate the role of TUFT1 in pulmonary fibrosis, we examined fibrotic responses after the silenced TUFT1 expression by using Adeno-associated virus knockdown of TUFT1 (*Tuft1*/short hairpin RNA (shRNA)) in bleomycin-induced mouse pulmonary fibrosis model. The schematic diagram illustrated the time and course of the experiments in Fig. 2A. Briefly, the mice were divided in four groups randomly, first, by intratracheal administration AAV shRNA NC/Tuft1 at the beginning, 7 days later, generated the mouse pulmonary fibrosis by bleomycin and labeled this time as the 0 day, and finally sacrificed the mice in 14th day. Interestingly the mice pulmonary imaging changes were presented in 14th day, the bleomycin treatment cause obvious pulmonary fibrosis change, and the *Tuft1*/shRNA alleviated the fibrotic intensity as detected by the Micro-CT scan (Fig. 2B). Moreover, mice treated with *Tuft1*/shRNA adenovirus showed normal lung tissues structure compared with the bleomycin group as detected by H&E staining in the first line of Fig. 2C. Meanwhile, the Masson's trichrome staining showed that the collagen deposition increased obviously in bleomycin groups, whereas this phenomenon could be rectified by disruption of TUFT1 in the second line of Fig. 2C, furthermore, silencing the Tuft1 reduced the expression of α-SMA as indicated by immunohistochemistry staining in the third line of Fig. 2C. According to Fig. 2C and Supplementary Fig. 1, bleomycin treated group increased the Ashcroft histopathological grading score, while silencing the Tuft1 decreased the Ashcroft histopathological grading score significantly in Fig. 2D. As expected, the bleomycin treatment enhanced the level of Hydroxyproline significantly, and the *Tuft1*/shRNA alleviated this phenomenon (Fig. 2E). Meanwhile the levels of Fibronectin and Collagen I were decreased by *Tuft1*/shRNA in pulmonary fibrosis process (Fig. 2F-I). In summary, these findings provide compelling evidence of the significant contribution of TUFT1 to the progression of pulmonary fibrosis. Moreover, the inhibition of TUFT1 has been demonstrated to alleviate bleomycin-induced lung fibrosis *in vivo*. Interestingly, the Phalloidin staining revealed a marked abundance of F-actin within the

fibrotic tissues of the bleomycin-induced lung fibrosis model, whereas the downregulation of Tuft1 via shRNA led to a reduction in F-actin formation within bleomycin-exposed lung tissues (Supplementary Fig. 2).

3.3 Blockade of TUFT1 inhibited fibrotic phenotype of epithelial cells and fibroblasts in vitro

Next, we intend to explore the influence of TUFT1 on the fibrotic phenotype of epithelial cells and fibroblasts *in vitro*. First of all, we evaluated the impact of si-TUFT1 on A549 cells as shown in Fig. 3A. Interestingly phalloidin staining revealed that the silencing of TUFT1 influence the microfilaments morphology of the A549 cells (Fig. 3B). Moreover, silencing TUFT1 slowed down the migration of the A549 as shown in Fig. 3C,D. Meanwhile, the knockdown of TUFT1 also reduce invasion of the A549 detected by transwell (Fig. 3E,F). In parallel, we also found that the silencing of TUFT1 influence the microfilaments morphology of the MRC-5 cells detected by phalloidin staining (Fig. 3G). As expected, knockdown of TUFT1 could decrease the expression of Fibronectin, Collagen , α-SMA and N-cadherin in MRC-5 cells (Fig. 3H). Also, silencing TUFT1 could slow down the migration progression of the MRC-5 as expected (Fig. 3I,J). Finally, we found that knocking down TUFT1 could decrease the gap of matrigel contraction in MRC-5 cells (Fig. 3K,L). These data implicated that disruption of TUFT1 suppresses the activation of both epithelial cells and fibroblasts *in vitro*.

3.4 N-WASP is indispensable in TUFT1 mediated pro-fibrotic phenotype

As silencing of the TUFT1 distorted the shape of microfilaments, in order to illustrate the mechanism of TUFT1 influence the microfilaments, we exam the expression level of N-WASP and p^{Y256}N-WASP, which influenced the assembly of cell microfilaments. Interestingly, the p^{Y256}N-WASP was decreased significantly by silencing TUFT1 in A549 cells (Fig. 4A,B.C). N-WASP and p^{Y256}N-WASP were showed a high expression as indicated by immunohistochemistry staining in IPF compare with the control (Fig. 4D, 4E). At the same time, N-WASP and p^{Y256}N-WASP were increased significantly in bleomycin induced fibrosis mice model compare with the control (Fig. 4F,G).

In order to ascertain whether the p^{Y256}N-WASP plays an important role in the progress of TUFT1 hamper the expression of fibrosis markers in MRC-5 cells, we used Sodium orthovanadate (SOV, 20μM), a phosphorylase inhibitor of Tyrosine, to interfere the expression level of p^{Y256}N-WASP after the silenced of TUFT1 for 48 hours, the result indicated that silencing the TUFT1 in MRC-5 cells could slow down matrigel contraction compare to the control, and Sodium orthovanadate reversed this phenomenon (Fig. 4H,I). In parallel, silenced the TUFT1 could decrease the expression of p^{Y256}N-WASP in TGF-β treated MRC-5 cells, meanwhile the fibrosis marker α-SMA was reduced, and the Sodium orthovanadate could relieve the decrease of the p^{Y256}N-WASP and the α-SMA (Fig. 4J-M).

3.5 TUFT1 interacted with N-WASP and mediated the phosphorylation of N-WASP

To explore the relationship between TUFT1 and N-WASP in epithelial cells, we constructed a vector of N-WASP. Over-expressed N-WASP led to a substantial increase in TUFT1 fluorescence intensity within A549 cells, and the N-WASP and TUFT1 expressed a perfect co-localization (Fig. 5A). Furthermore, we found that exogenously expressed N-WASP and TUFT1 co-immunoprecipitated in HEK293T cells (Fig. 5B), and exogenously TUFT1 and N-WASP also co-immunoprecipitated in HEK293T cells (Fig. 5C). Interestingly, we upregulate the TUFT1 in A549 cells, the expression of p^{Y256}N-WASP was increased obviously (Fig. 5D). Meanwhile, the disperse phenomena of p^{Y256}N-WASP were appeared in the TGF-β (5 nM) induced cells model. We examine the location of p^{Y256}N-WASP in the TGF-β induced A549 cells, and confirmed that silencing the TUFT1 rendered the p^{Y256}N-WASP keep away from the nucleus compare to the control detected by immunofluorescent staining (Fig. 6E), the distance of p^{Y256}N-WASP to the core of the nucleus were measured (Fig. 6F), and this phenomenon attribute to the microfilament destruction in A549 cells. Collectively, these above results show that TUFT1 interacts with N-WASP and influence the level and location of p^{Y256}N-WASP

3.6 TUFT1 mediates the formation of stress fiber in a p^{Y256} N-WASP dependent manner

As is known that N-WASP play a critical role in regulating the formation of α-SMA-containing cytoplasmic filaments during myofibroblast differentiation and in myofibroblast contractility, p^{Y256}N-WASP is the active form of the N-WASP, which can active the ARP2/3 complex [24]. To explore the mechanism of TUFT1 regulate p^{Y256}N-WASP in the progress of fibrosis, we found bleomycin could induce a high expression of p^{Y256}N-Wasp, whereas silencing the Tuft1 could decrease the expression of p^{Y256}N-Wasp and collagen in mice model (Fig. 6A,B). In parallel, the bleomycin could induce a high expression of p^{Y256}N-WASP and silencing the Tuft1 could decrease the expression of p^{Y256}N-Wasp in mice model as detected by immunohistochemistry staining, meanwhile, we found silencing the Tuft1 could disperse the p^{Y256}N-Wasp in the fibrosis foci cells (Supplementary Fig. 3).

TUFT1 was engaged in the formation of microfilaments and silence the TUFT1 could decrease the percentage of cells with actin cores in A549 cells, which is similar to the effect of wiskostatin, a selective N-WASP inhibitor which can bind the GTPase binding domain stabilizing the autoinhibited conformation (Fig. 6C,D).

Next, we selected the Wiskostatin (50 μM) to prevent the activation of Arp2/3 complex in the actin cytoskeleton. Interestingly, over-expressed TUFT1 could make the p^{Y256}N-WASP distributed more closely to the core of the nucleus in MRC-5 cells, whereas the Wiskostatin could reverse this phenomenon completely (Supplementary Fig. 4). Meanwhile, over-expressed the TUFT1 in MRC-5 cells could accelerate the matrigel contraction, and Wiskostatin could delay it (Fig. 6E,F). Interestingly in MRC-5 cells, over-

expressed TUFT1 can induce a high expression of p^{Y256}N-WASP and more fibrosis marker FN, collagen and α-SMA, while N-WASP inhibitor wiskostatin could reverse this phenomenon detected by western-blot (Fig. 6G-K).

These above data illustrated that TUFT1 facilitates lung fibrosis in a p^{Y256}N-WASP-dependent manner.

4 Discussion

IPF is a complex and chronic disease influenced by multiple factors, including genetic and environmental risks [29]. One crucial aspect of the pathogenic process is the dysfunction of lung epithelium, which triggers a cascade of events involving growth factors, cytokines, and extracellular matrix signaling. These pathways activate various repair processes that lead to inflammatory cell recruitment, fibroblast proliferation, and extracellular matrix expansion, ultimately resulting in tissue fibrosis [30, 31]. However, the specific mechanisms underlying pulmonary fibrosis remain unclear.

Bleomycin administration is the most commonly used method to induce pulmonary fibrosis in animal models [32, 33]. TUFT1 has been implicated in several physiological and pathological processes, such as adaptation to hypoxia, promotion of tumor growth and metastasis[13, 15, 34], and involvement in neurotrophin-mediated neuronal differentiation [35]. In our present investigation, a marked elevation of TUFT1 was observed in both models of pulmonary fibrosis and in the context of pulmonary transformation induced by TGF-β1. These findings collectively imply a potential implication of TUFT1 in the development of this disease.

TGF-β1 is a pro-fibrotic factor which capable of eliciting epithelial-mesenchymal transformation and fibroblast activation, resulting in abnormal ECM accumulation and poor compliance of lung tissue [36–38]. In this study, we found TUFT1 is induced by TGF-β1 in both epithelial cells and fibroblasts. The attenuation of pro-fibrotic characteristics in both cell types upon TUFT1 loss suggests its involvement in mediating the TGF-β1-induced phenotypic transition of cells.

In previous studies, TUFT1 was found to influence the assembly of microfilaments in A549 cells [16], while N-WASP was identified as an important regulator of the cytoskeleton that stimulates Arp2/3-mediated actin nucleation [39]. Further investigations revealed that the N-WASP-Arp2/3 pathway was activated in both mice pulmonary fibrosis models induced by bleomycin and specimens from the lung of IPF patients [40]. N-WASP is critical for the formation of α-SMA filaments during the differentiation of myofibroblasts, and TGF-β1 is necessary for the activation of N-WASP [24]. It was also reported that TGF-β1 induces stress fiber formation in vascular smooth muscle cells [41]. In addition, repeated lung injury can lead to the accumulation of ECM and stress fiber formation, which reduces the plasticity of lung tissue and increases the stress of fibrosis tissue. Based on these findings, we hypothesize that N-WASP-induced stress fiber may be a factor promoting fibrosis. This study illustrated that the level of p^{Y256}N-WASP was increased significantly in TGF-β1 treated fibroblasts and that TUFT1 interacted with N-WASP in 293T cells as evidenced by Co-IP. Moreover, silencing TUFT1 hampered TGF-β1-induced

phosphorylation of N-WASP at tyrosine residue 256 (Y256) both *in vitro* and *in vivo*, and p^{Y256}N-WASP was markedly upregulated in the TUFT1 over-expression group compared to the control, which could activate the Arp2/3 complex, and this activation could be inhibited by wiskostatin [16]. Our findings suggest that TUFT1 mediates the mechanical stress in pulmonary fibrosis via N-WASP activation. This positive feedback results in tighter stress fibers in the cells engaged in the pathological process of IPF, and the mechanism provides a novel explanation of IPF, which progressively deteriorates continuously.

5 Conclusions

In conclusion, our data suggested that TUFT1 exerts pro-fibrotic effects by influencing stress fiber formation through promoting the phosphorylation of N-WASP in both epithelial and fibroblast cells (Fig. 7). Given these findings, TUFT1 represents a promising therapeutic target for the attenuation of pulmonary fibrosis. Future research aimed at developing interventions targeting TUFT1 may hold the key to more effective treatments for this devastating lung condition.

Declarations

Acknowledgments

This study was supported by the Ministry of Science and Technology, PR China, 2019YFE0119500, Henan Province Science and Technology Project 222102310711, Xinxiang Major Project 21ZD002, and the 111 Project “State Innovation Base for Pulmonary Fibrosis”.

Author contributions

Conceptualization, G.Y. and C.N.; methodology, C.N., K.X.; software, Y.H.; validation, Y.J., X.P., and Y.L.; data analysis, C.N., Y.H., R.W., and H.L.; investigation, C.N.; resources, G.Y.; supervision, G.Y., X.P., and L.W.; original draft, C.N., K.X., and Y.H.; review and editing, Q.W., L.W., J.Y., and I.R.; project administration, G.Y.; funding acquisition, G.Y. All authors have read and approved the final article.

Compliance with ethics guidelines

The authors declare no conflict of interest.

All institutional and national guidelines for the care and use of laboratory animals were followed. Animal maintenance and handling procedures was approved by Henan Normal University Institutional Animal Care and Use Committee (IACUC, SMKX-2118BS1018). The human lung tissue study was approved by the Xinxiang central hospital Medical Research Ethics Committee (No.2019-01-12). The research conformed to the principles of the Helsinki Declaration

References

1. Heukels P, Moor CC, von der Thusen JH, Wijsenbeek MS, Kool M. Inflammation and immunity in IPF pathogenesis and treatment. Respir Med. 2019;147:79–91.
2. Yu G, Tzouvelekis A, Wang R, Herazo-Maya JD, Ibarra GH, Srivastava A, de Castro JPW, Deluliis G, Ahangari F, Woolard T, et al. Thyroid hormone inhibits lung fibrosis in mice by improving epithelial mitochondrial function. Nat Med. 2018;24:39–49.
3. Chanda D, Otoupalova E, Smith SR, Volckaert T, De Langhe SP, Thannickal VJ. Developmental pathways in the pathogenesis of lung fibrosis. Mol Aspects Med. 2019;65:56–69.
4. Ballester B, Milara J, Cortijo J. Idiopathic Pulmonary Fibrosis and Lung Cancer: Mechanisms and Molecular Targets. Int J Mol Sci 2019, 20.
5. Shenderov K, Collins SL, Powell JD, Horton MR. Immune dysregulation as a driver of idiopathic pulmonary fibrosis. J Clin Invest 2021, 131.
6. Sundarakrishnan A, Chen Y, Black LD, Aldridge BB, Kaplan DL. Engineered cell and tissue models of pulmonary fibrosis. Adv Drug Deliv Rev. 2018;129:78–94.
7. Richeldi L, Collard HR, Jones MG. Idiopathic pulmonary fibrosis. The Lancet. 2017;389:1941–52.
8. Juge PA, Crestani B, Dieude P. Recent advances in rheumatoid arthritis-associated interstitial lung disease. Curr Opin Pulm Med. 2020;26:477–86.
9. Parimon T, Yao C, Stripp BR, Noble PW, Chen P. Alveolar Epithelial Type II Cells as Drivers of Lung Fibrosis in Idiopathic Pulmonary Fibrosis. Int J Mol Sci 2020, 21.
10. Maghsoudloo M, Azimzadeh Jamalkandi S, Najafi A, Masoudi-Nejad A. An efficient hybrid feature selection method to identify potential biomarkers in common chronic lung inflammatory diseases. Genomics. 2020;112:3284–93.
11. Deutsch D, Leiser Y, Shay B, Fermon E, Taylor A, Rosenfeld E, Dafni L, Charuvi K, Cohen Y, Haze A, et al. The human tuftelin gene and the expression of tuftelin in mineralizing and nonmineralizing tissues. Connect Tissue Res. 2002;43:425–34.
12. Jeremias F, Koruyucu M, Kuchler EC, Bayram M, Tuna EB, Deeley K, Pierri RA, Souza JF, Fragelli CM, Paschoal MA, et al. Genes expressed in dental enamel development are associated with molar-incisor hypomineralization. Arch Oral Biol. 2013;58:1434–42.
13. Lin H, Zeng W, Lei Y, Chen D, Nie Z. Tuftelin 1 (TUFT1) Promotes the Proliferation and Migration of Renal Cell Carcinoma via PI3K/AKT Signaling Pathway. Pathol Oncol Res. 2021;27:640936.
14. Liu W, Han J, Shi S, Dai Y, He J. TUFT1 promotes metastasis and chemoresistance in triple negative breast cancer through the TUFT1/Rab5/Rac1 pathway. Cancer Cell Int. 2019;19:242.
15. Zhou B, Zhan H, Tin L, Liu S, Xu J, Dong Y, Li X, Wu L, Guo W. TUFT1 regulates metastasis of pancreatic cancer through HIF1-Snail pathway induced epithelial-mesenchymal transition. Cancer Lett. 2016;382:11–20.
16. Kawasaki N, Isogaya K, Dan S, Yamori T, Takano H, Yao R, Morishita Y, Taguchi L, Morikawa M, Heldin CH, et al. TUFT1 interacts with RABGAP1 and regulates mTORC1 signaling. Cell Discov. 2018;4:1.

17. Knipe RS, Tager AM, Liao JK, Ishikawa Y. The Rho Kinases: Critical Mediators of Multiple Profibrotic Processes and Rational Targets for New Therapies for Pulmonary Fibrosis. Pharmacol Rev. 2015;67:103–17.
18. Pegoraro AF, Janmey P, Weitz DA. Mechanical Properties of the Cytoskeleton and Cells. Cold Spring Harb Perspect Biol 2017, 9.
19. Blain EJ. Involvement of the cytoskeletal elements in articular cartilage homeostasis and pathology. Int J Exp Pathol. 2009;90:1–15.
20. Svitkina TM. Ultrastructure of the actin cytoskeleton. Curr Opin Cell Biol. 2018;54:1–8.
21. Shi X, Tang D, Xing Y, Zhao S, Fan C, Zhong J, Cui Y, Shi K, Jiu Y. Actin nucleator formins regulate the tension-buffering function of caveolin-1. J Mol Cell Biol. 2022;13:876–88.
22. Zeng Y, Cao Y, Liu L, Zhao J, Zhang T, Xiao L, Jia M, Tian Q, Yu H, Chen S, Cai Y. SEPT9_i1 regulates human breast cancer cell motility through cytoskeletal and RhoA/FAK signaling pathway regulation. Cell Death Dis. 2019;10:720.
23. Katanov C, Novak N, Vainshtein A, Golani O, Dupree JL, Peles E. N-Wasp Regulates Oligodendrocyte Myelination. J Neurosci. 2020;40:6103–11.
24. Cai GQ, Chou CF, Hu M, Zheng A, Reichardt LF, Guan JL, Fang H, Luckhardt TR, Zhou Y, Thannickal VJ, Ding Q. Neuronal Wiskott-Aldrich syndrome protein (N-WASP) is critical for formation of alpha-smooth muscle actin filaments during myofibroblast differentiation. Am J Physiol Lung Cell Mol Physiol. 2012;303:L692–702.
25. Koch J, Schober SJ, Hindupur SV, Schöning C, Klein FG, Mantwill K, Ehrenfeld M, Schillinger U, Hohnecker T, Qi P et al. Targeting the Retinoblastoma/E2F repressive complex by CDK4/6 inhibitors amplifies oncolytic potency of an oncolytic adenovirus. Nat Commun 2022, 13.
26. Wang L, Xu K, Wang N, Ding L, Zhao W, Wan R, Zhao W, Guo X, Pan X, Yang J et al. Fenbendazole Attenuates Bleomycin-Induced Pulmonary Fibrosis in Mice via Suppression of Fibroblast-to-Myofibroblast Differentiation. Int J Mol Sci 2022, 23.
27. Yang D, Xu P, Su H, Zhong W, Xu J, Su Z, Liu X. The histone methyltransferase DOT1L is a new epigenetic regulator of pulmonary fibrosis. Cell Death Dis. 2022;13:60.
28. Yu G, Kovkarova-Naumovski E, Jara P, Parwani A, Kass D, Ruiz V, Lopez-Otin C, Rosas IO, Gibson KF, Cabrera S, et al. Matrix metalloproteinase-19 is a key regulator of lung fibrosis in mice and humans. Am J Respir Crit Care Med. 2012;186:752–62.
29. Hewlett JC, Kropski JA, Blackwell TS. Idiopathic pulmonary fibrosis: Epithelial-mesenchymal interactions and emerging therapeutic targets. Matrix Biol. 2018;71–72:112–27.
30. Glass DS, Grossfeld D, Renna HA, Agarwala P, Spiegler P, DeLeon J, Reiss AB. Idiopathic pulmonary fibrosis: Current and future treatment. Clin Respir J. 2022;16:84–96.
31. Spagnolo P, Kropski JA, Jones MG, Lee JS, Rossi G, Karampitsakos T, Maher TM, Tzouvelekis A, Ryerson CJ. Idiopathic pulmonary fibrosis: Disease mechanisms and drug development. Pharmacol Ther. 2021;222:107798.

32. Carrington R, Jordan S, Wong YJ, Pitchford SC, Page CP. A novel murine model of pulmonary fibrosis: the role of platelets in chronic changes induced by bleomycin. J Pharmacol Toxicol Methods. 2021;109:107057.
33. Shamskhou EA, Kratochvil MJ, Orcholski ME, Nagy N, Kaber G, Steen E, Balaji S, Yuan K, Keswani S, Danielson B, et al. Hydrogel-based delivery of Il-10 improves treatment of bleomycin-induced lung fibrosis in mice. Biomaterials. 2019;203:52–62.
34. Dou C, Zhou Z, Xu Q, Liu Z, Zeng Y, Wang Y, Li Q, Wang L, Yang W, Liu Q, Tu K. Hypoxia-induced TUFT1 promotes the growth and metastasis of hepatocellular carcinoma by activating the Ca(2+)/PI3K/AKT pathway. Oncogene. 2019;38:1239–55.
35. Shilo D, Cohen G, Blumenfeld A, Goren K, Hanhan S, Sharon S, Haze A, Deutsch D, Lazarovici P. Tuftelin Is Required for NGF-Induced Differentiation of PC12 Cells. J Mol Neurosci. 2019;68:135–43.
36. Zhang C, Zhu X, Hua Y, Zhao Q, Wang K, Zhen L, Wang G, Lu J, Luo A, Cho WC, et al. YY1 mediates TGF-beta1-induced EMT and pro-fibrogenesis in alveolar epithelial cells. Respir Res. 2019;20:249.
37. Wu G, Xie B, Lu C, Chen C, Zhou J, Deng Z. microRNA-30a attenuates TGF-beta1-induced activation of pulmonary fibroblast cell by targeting FAP-alpha. J Cell Mol Med. 2020;24:3745–50.
38. Liu G, Philp AM, Corte T, Travis MA, Schilter H, Hansbro NG, Burns CJ, Eapen MS, Sohal SS, Burgess JK, Hansbro PM. Therapeutic targets in lung tissue remodelling and fibrosis. Pharmacol Ther. 2021;225:107839.
39. Kovacs EM, Verma S, Ali RG, Ratheesh A, Hamilton NA, Akhmanova A, Yap AS. N-WASP regulates the epithelial junctional actin cytoskeleton through a non-canonical post-nucleation pathway. Nat Cell Biol. 2011;13:934–43.
40. Yan P, Liu J, Zhou R, Lin C, Wu K, Yang S, Yang S, Zhou J, Xu L, Wang H, Zhao L. LASP1 interacts with N-WASP to activate the Arp2/3 complex and facilitate colorectal cancer metastasis by increasing tumour budding and worsening the pattern of invasion. Oncogene. 2020;39:5743–55.
41. Park S, Lee S, Park EJ, Kang M, So I, Jeon JH, Chun JN. TGFbeta1 induces stress fiber formation through upregulation of TRPC6 in vascular smooth muscle cells. Biochem Biophys Res Commun. 2017;483:129–34.

Figures

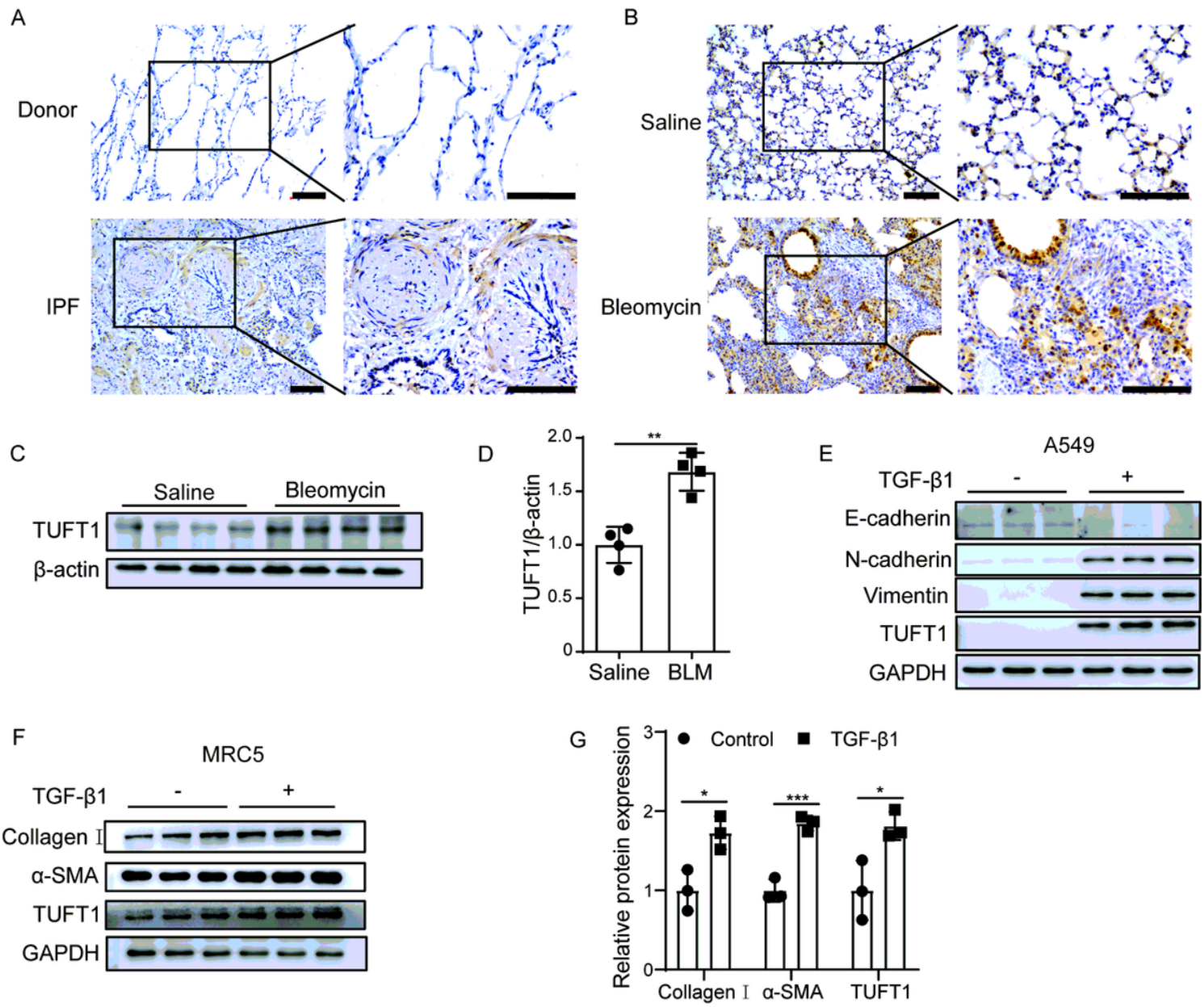

Figure 1

TUFT1 was increased in IPF and pulmonary fibrosis models. (A) Representative immunohistochemistry staining of TUFT1 in the lung sections from the Donor and IPF patient, TUFT1 was mainly expressed in epithelial and fibroblast cells in the fibrosis foci of IPF lung sections, scale bars:100 μm. (B) TUFT1 was high expressed in bleomycin induced fibrosis model, and mainly expressed in epithelial and fibroblast cells compare to the control, scale bars:100 μm. (C) TUFT1 was increased in pulmonary fibrosis models *in vivo* detected by Western blot. (D) Densitometry analysis of fig C (mean ± SD). (E) TUFT1 was increased significantly in TGF-β1-induced A549 cells in vitro detected by Western blot. (F) TUFT1, collagen I and α-SMA were increased obviously in TGF-β1-induced MRC-5 cells detected By Western blot. (G) Densitometry analysis of fig f (mean ± SD). * $P < 0.05$, ** $P < 0.01$, *** $P < 0.001$, and **** $P < 0.0001$.

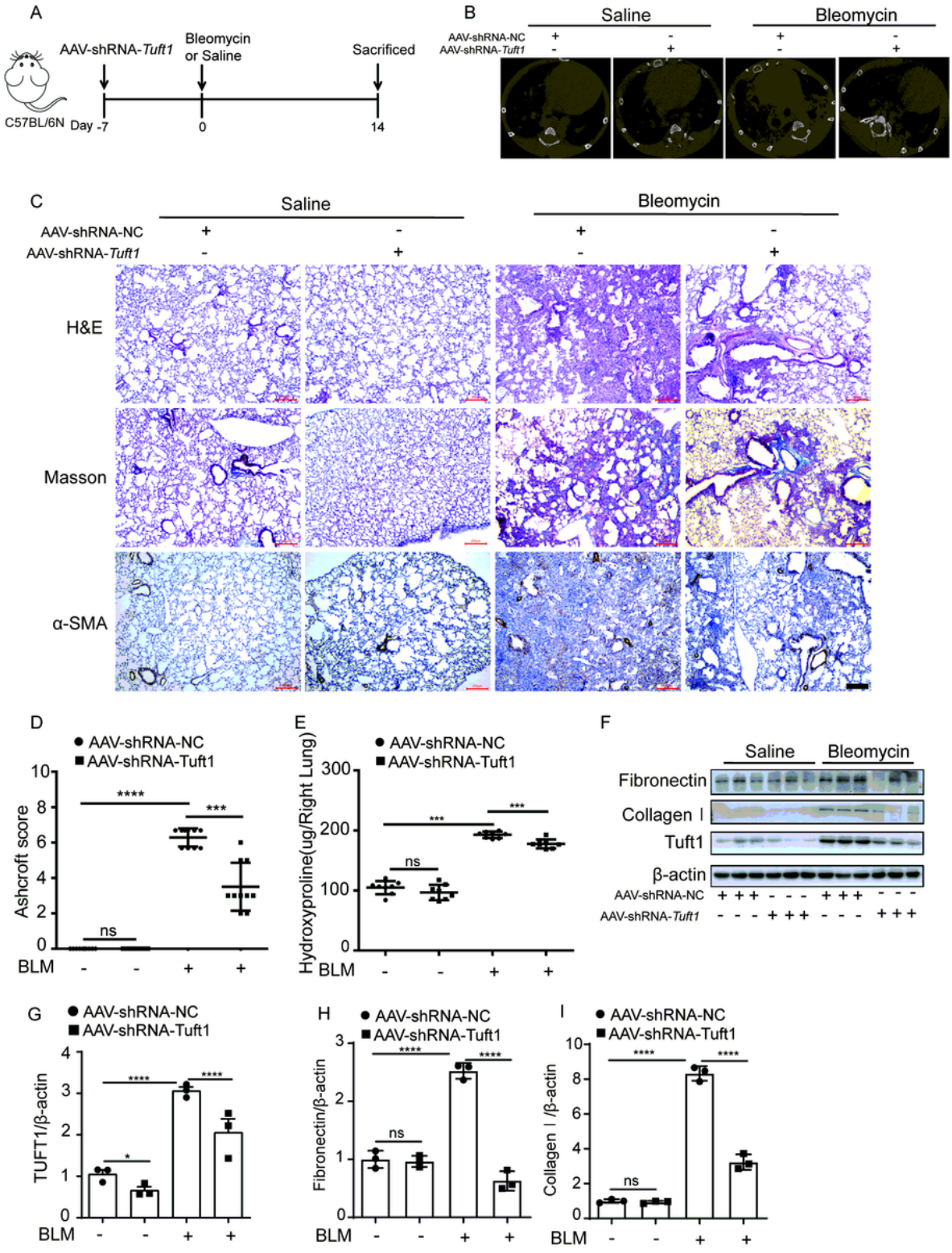

Figure 2

TUFT1 disruption inhibited bleomycin-induced mouse pulmonary fibrosis *in vivo*. (A) Schematic diagram illustrated the time and course of the experiments(B) The pulmonary images of mice detected by Micro-CT scan in 14th day. (C) Representative images of H&E staining, Masson's trichrome staining of the lung section and Immunohistochemical staining images of α−SMA, scale bars: 200 μm. (D) Ashcroft score (mean ± SD). (E) Quantitative hydroxyproline assay of the right lung (mean ± SD, n = 8 mice per group).

(F) Western blotting assay of FN, collagen I and Tuft1 in the lung homogenate; β-actin used as the loading control. (G-I) Corresponding optical densitometry analysis of (F) (mean ± SD). * P< 0.05, ** P < 0.01, *** P<0.001, and **** P< 0.0001.

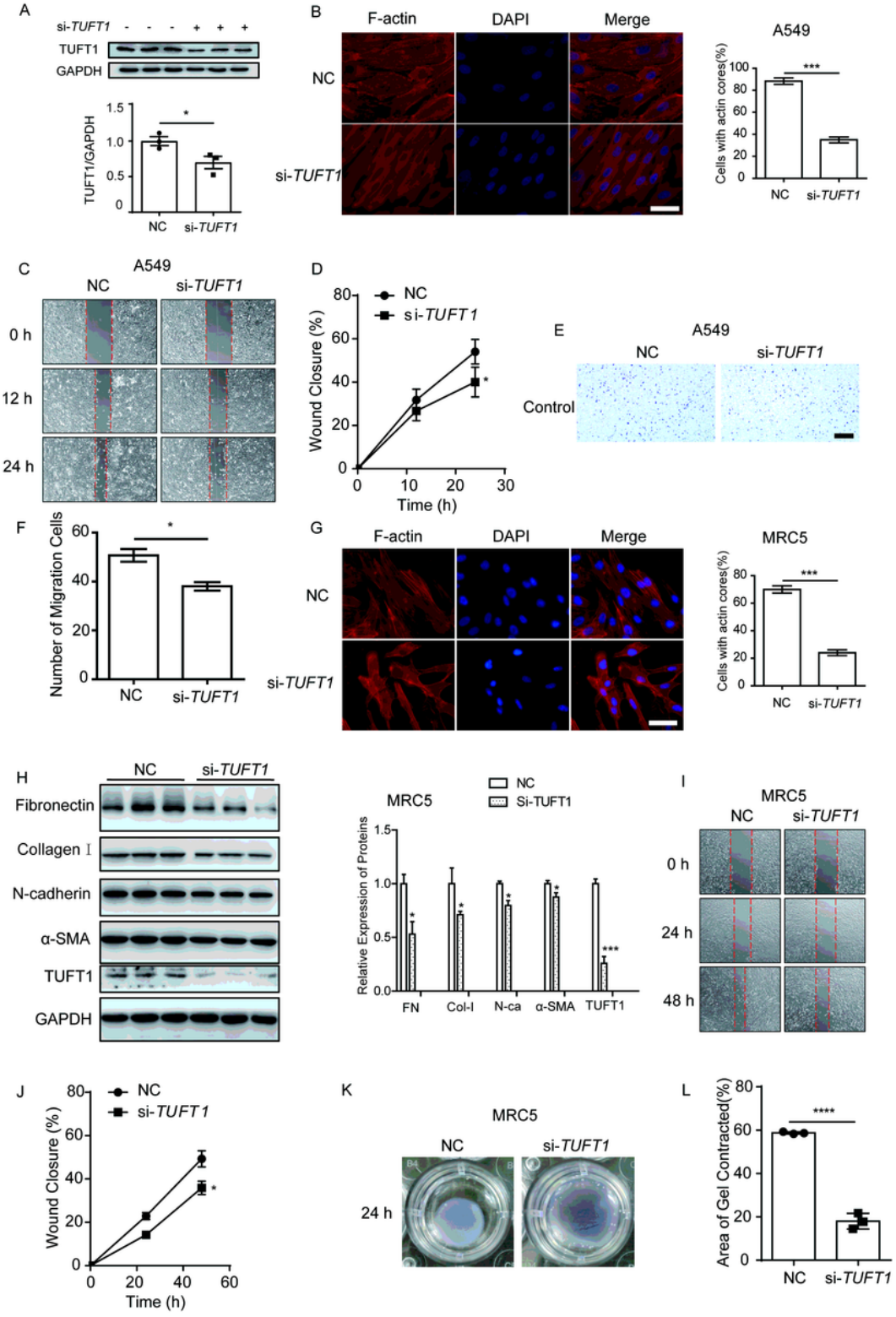

Figure 3

Blockade of TUFT1 inhibited TGF-β1-induced fibrosis *in vitro*. (A) Interference efficiency of TUFT1 in the A549 cells detected by Western blotting. (B) The microfilaments morphology of the A549 cells were revealed by the phalloidin staining in si-TUFT1 groups and control, scale bars: 10 μm. F-actin was quantified by the percentage of the cells with the actin cores. (C,D) The wound healing progression of A549 cells in si-TUFT1 groups and control. (E,F) The migration ability of A549 cells in si-TUFT1 groups and control, scale bars: 1 mm. (G) The microfilaments morphology of the MRC-5 cells was revealed by the phalloidin staining in si-TUFT1 groups and control, scale bars: 100 μm. F-actin was quantified by the percentage of the cells with the actin cores. (H) Knockdown of TUFT1 could decrease the expression of FN, Collagen Ⅰ, α-SMA and N-cadherin in TGF-β1-induced MRC-5 cells. (I,J) The wound healing progression of MRC-5 cells in si-TUFT1 groups and control. (K,L) The extent of matrigel contraction in MRC-5 cells in si-TUFT1 groups and control. * $P< 0.05$, ** $P < 0.01$, *** $P<0.001$, and **** $P< 0.0001$.

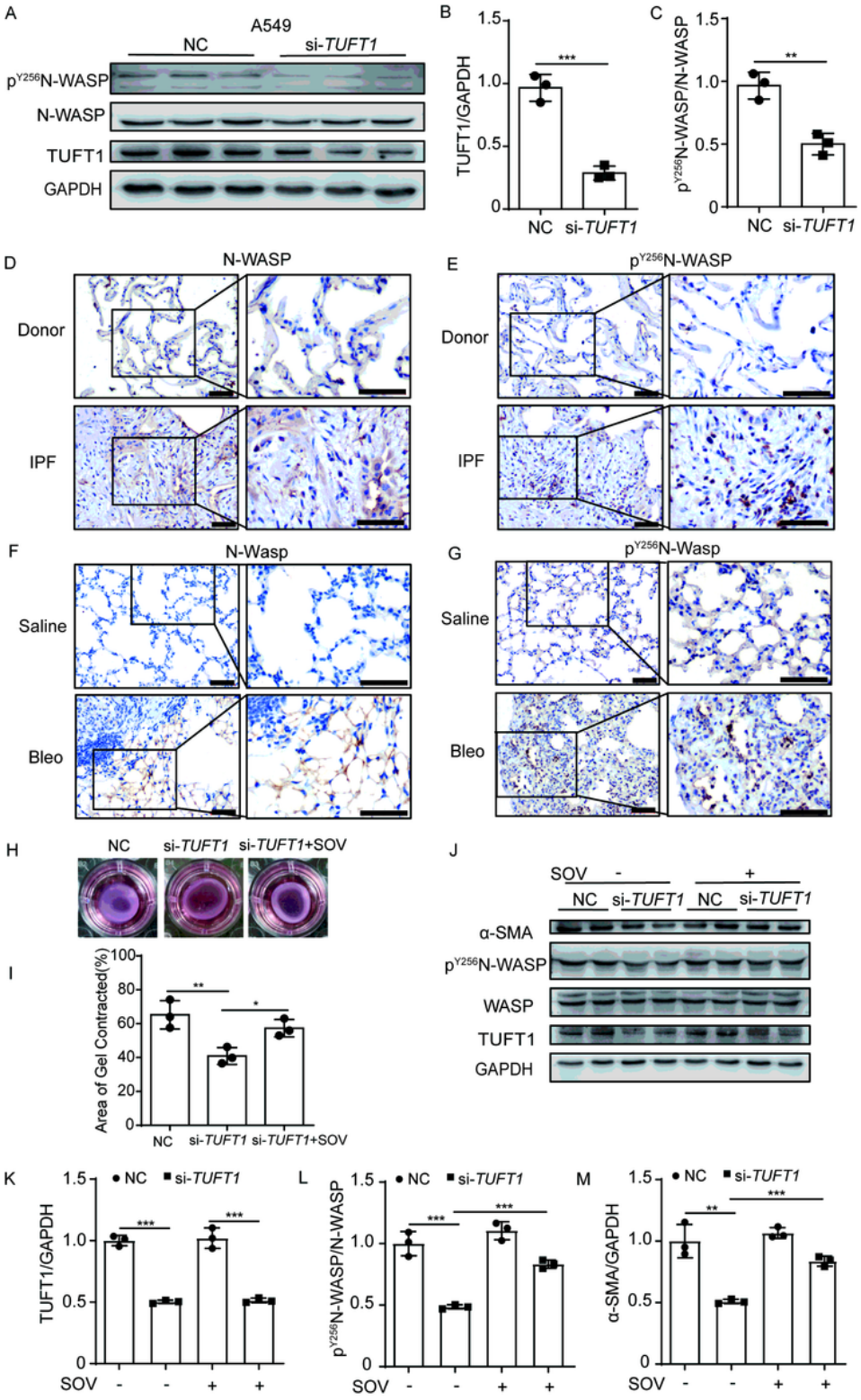

Figure 4

N-WASP played an important role in the progress of TUFT1 interfering with fibrosis. (A-C) Knockdown of TUFT1 can inhibited the phosphorylation level of N-WASP in A549 cells. (D) Immunohistochemical staining of N-WASP in IPF lung tissue compare to the donor. (E) Immunohistochemical staining of p^{Y256}N-WASP in IPF lung tissue compare to the donor. (F) Immunohistochemical stain images of N-Wasp in bleomycin induced fibrosis lung tissue compare to the control. (G) Immunohistochemical stain images

of p^{Y256}N-Wasp in bleomycin induced fibrosis lung tissue compare to the control, scale bars: 50 μm. (H,I) Silence the TUFT1 in MRC-5 cells could slow down the matrigel contraction compare to the control, and the Sodium orthovanadate could reverse this phenomenon. (J) Silence the TUFT1 could decrease the expression of p^{Y256}N-WASP and α-SMA, the Sodium orthovanadate could relieve the decrease level of p^{Y256}N-WASP and α-SMA. (K-M) Corresponding optical densitometry analysis of J (mean ± SD). * P< 0.05, ** P < 0.01, and *** P<0.001.

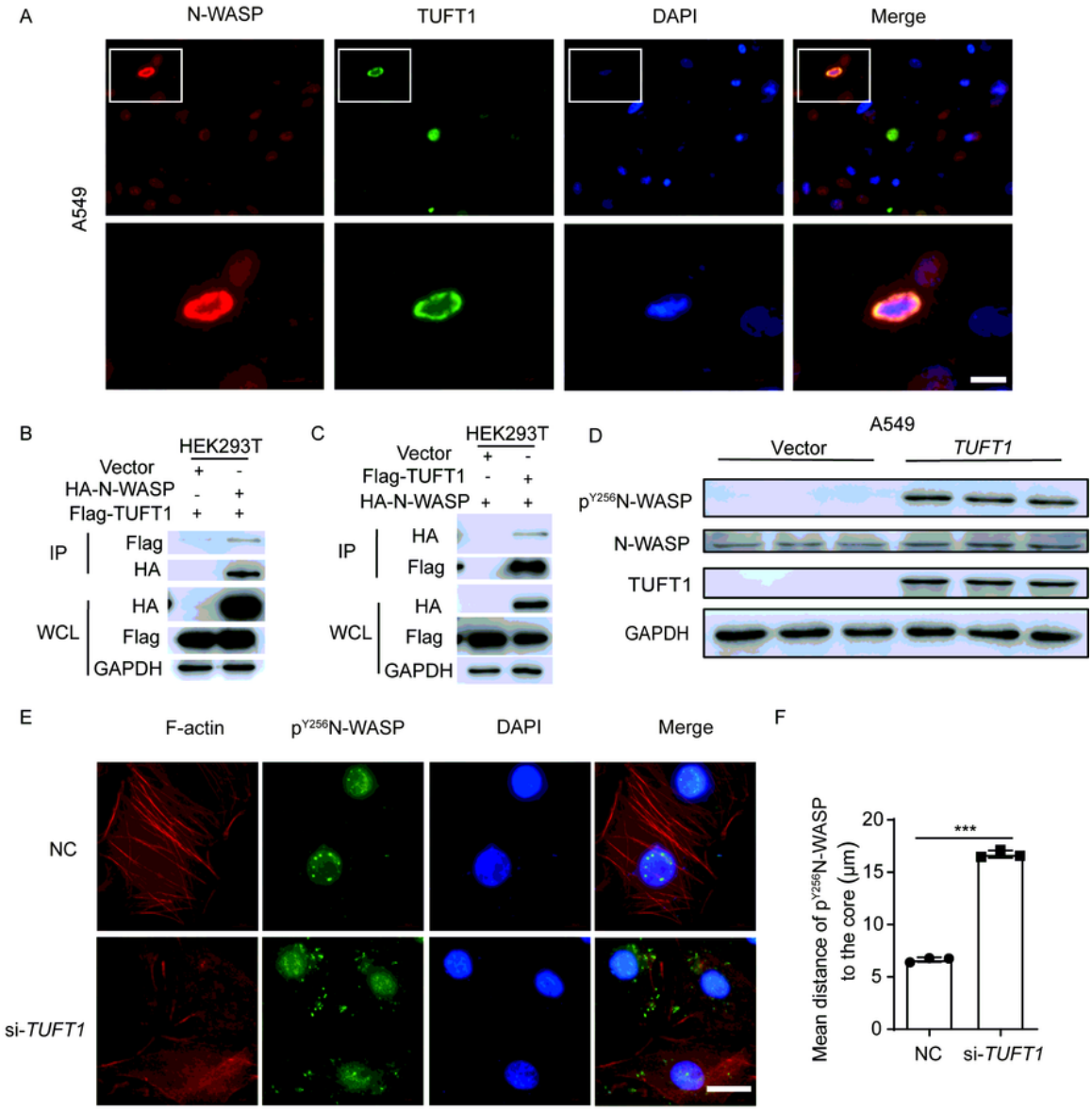

Figure 5

TUFT1 interacted with N-WASP and affected the expression of p^{Y256}N-WASP. (A) N-WASP and TUFT1 appeared a perfect co-localization in A549 cells detected by immunofluorescent staining, scale bars: 10 μm. (B) Exogenously expressed N-WASP and TUFT1 co-immunoprecipitated in HEK293T cells. (C) Exogenously TUFT1 and N-WASP have fine co-immunoprecipitated inHEK293T cells. (D) TUFT1 can induce a highly expression of p^{Y256}N-WASP in A549 cells. (E) Silencing the TUFT1 could make the p^{Y256}N-WASP keep away from the nucleus compare to the control detected by immunofluorescent staining, scale bars: 20 μm. (F) The distance of p^{Y256}N-WASP to the core of the nucleus was quantified.

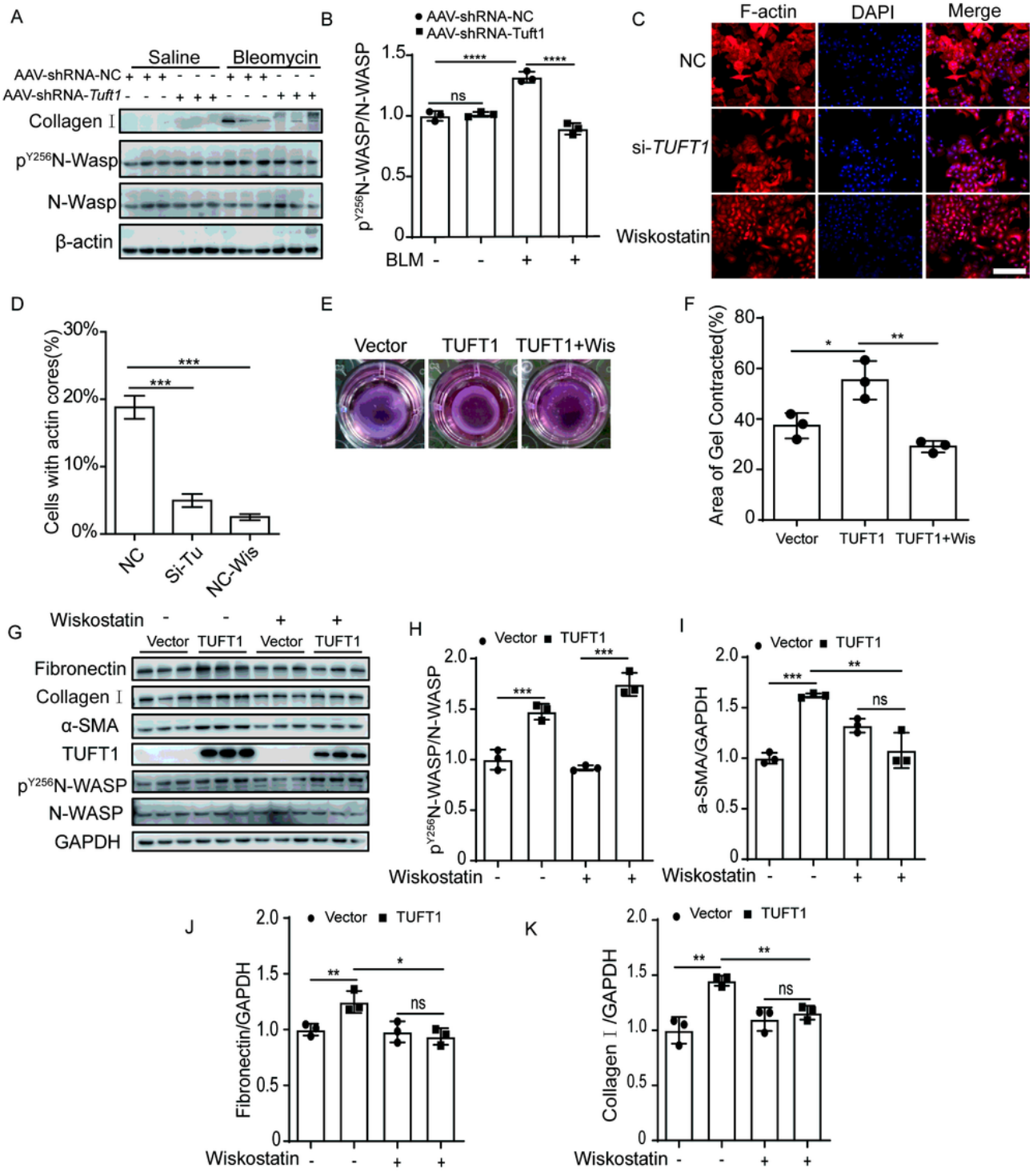

Figure 6

TUFT1 mediated lung fibrosis in p^{Y256}N-WASP dependent manner. (A) Western blotting assay of p^{Y256}N-WASP, N-WASP and collagen I in the lung homogenate; β-actin used as the loading control. (B) The relative expression of p^{Y256}N-WASP/N-WASP. (C) The expression of F-actin in si-TUFT1 group, wiskostatin group and control detected by Phalloidin staining in A549 cells, scale bars: 200 μm. (D) The percentage of cells with actin cores in A549 according to (c). (E,F) Over-expressed the TUFT1 in MRC-5 cells could

accelerate the matrigel contraction, and Wiskostatin could delay this phenomenon. (G) Over-expressed TUFT1 induced expression of p^{Y256}N-WASP and fibrosis marker FN, collagen Ⅰ and α-SMA, while wiskostatin could reverse this phenomenon detected by western-blot. (H-K) Corresponding optical densitometry analysis of (G) (mean ± SD). * *P*< 0.05, ** *P* < 0.01, *** *P*<0.001, and **** *P*< 0.0001.

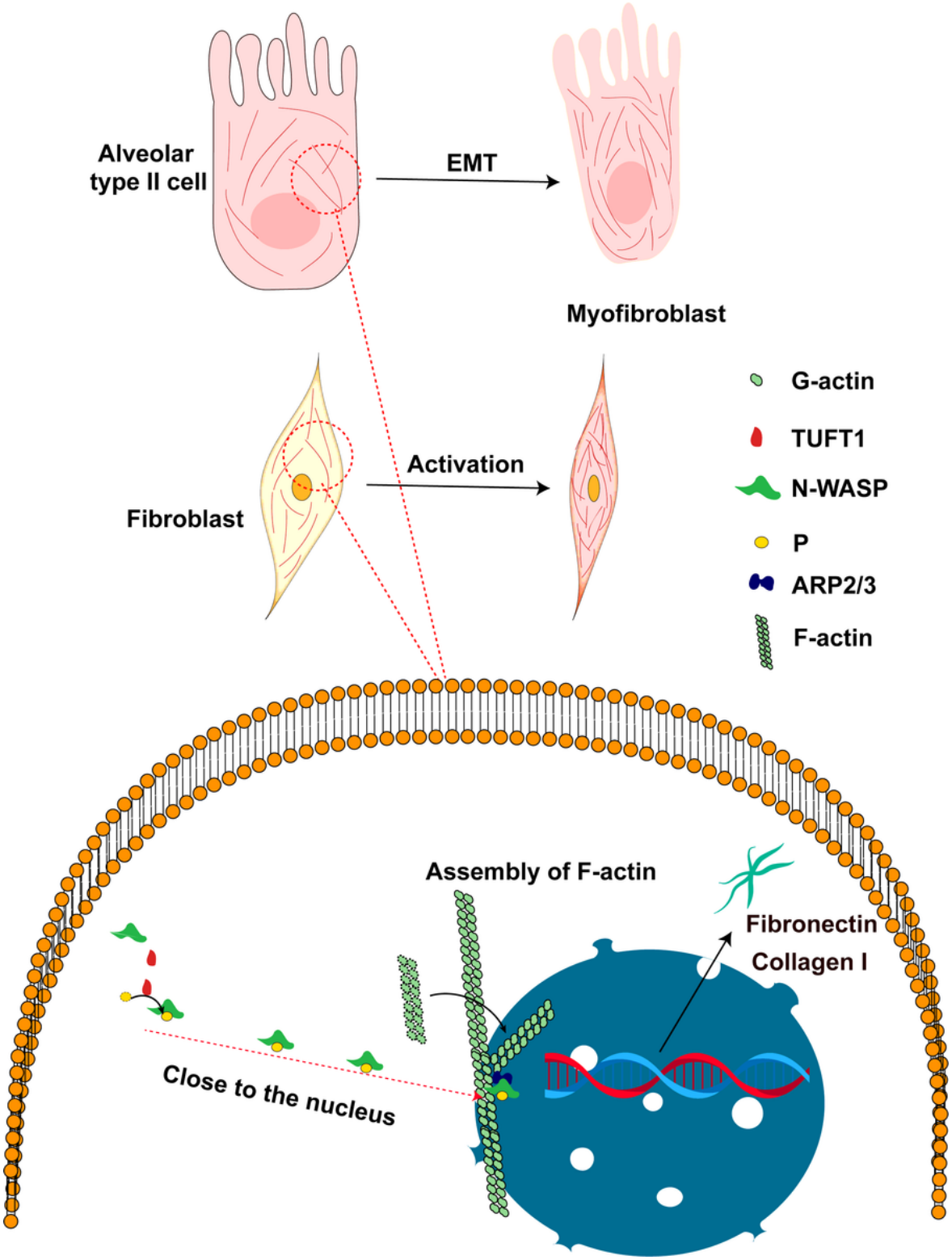

Figure 7

Schematic Representation of TUFT1 Involvement in the Pathophysiological Processes of Pulmonary Fibrosis. Our study has unveiled a schematic model elucidating the role of TUFT1 in the pathophysiological processes underlying pulmonary fibrosis. Specifically, our data demonstrate that TUFT1 orchestrates the translocation of pY256N-WASP into the cell nucleus, which facilitates the assembly of actin filaments, culminating in the enhanced formation of stress fibers. This heightened TUFT1-induced stress fiber formation appears to drive the cellular phenotypic transition towards a pro-fibrotic state.

Supplementary Files

This is a list of supplementary files associated with this preprint. Click to download.

- SupplementaryFig1.tif
- SupplementaryFig2.tif
- supplementaryFig3.tif
- supplementaryFig4.tif
- Originalfulllengthwesternblots20230901173207.pdf